

## Numerical study of a PCM-air heat exchanger's thermal performance

F Herbinger, M Bhourri and D Groulx<sup>1</sup>

Mechanical Engineering Department, Dalhousie University, Halifax, NS, Canada

E-mail: dominic.groulx@dal.ca

**Abstract.** In this paper, the use of PCMs in HVAC applications is investigated by studying numerically the thermal performance of a PCM-air heat exchanger. The PCM used in this study is dodecanoic acid. A symmetric 3D model, incorporating conductive and convective heat transfer (air only) as well as laminar flow, was created in COMSOL Multiphysics 5.0. Simulations examined the dependence of the heat transfer rate on the temperature and velocity of the incoming air as well as the size of the channels in the heat exchanger. Results indicated that small channels size lead to a higher heat transfer rates. A similar trend was also obtained for high incoming air temperature, whereas the heat transfer rate was less sensitive to the incoming air velocity.

### 1. Introduction

Several studies of phase change material (PCM) – air heat exchanger designs for thermal energy storage in heating ventilation and air conditioning (HVAC) systems are found in the literature. These studies cover different heat exchanger configurations: parallel PCMs slabs with rectangular air flow channels in-between [1-11]; cross-flow heat exchangers where one [12] or multiple PCMs [13] filled tubes and air is driven across the tubes bank; single [14] or modular [15, 16] heat exchangers based on a shell and tubes design where the PCM is on the shell side and air is flowing either across the cylinder containing the PCM or through the tubes; and a cylindrical reactor where air passes through packed layers of spherical PCM capsules [17].

Among these various heat exchanger geometries, the one with PCM slabs and air gaps is the most studied for thermal energy storage in building ventilation systems. It has been the subject of intensive experimental development where real-scale prototypes have been built and tested [2, 5, 6, 9], and the results have been used to validate numerical analysis [5-7, 9] for further optimization of the heat storage system.

In this paper, a PCM-air heat exchanger configuration inspired in part from this previous work was modelled. However, a cellular structure where cubic PCM and air channels were alternated was considered. This configuration was adapted from the air-to-air heat exchanger design, typically used in heat recovery ventilation systems [18]. The main objective was to assess the thermal performance of such a heat exchanger design as a function of its geometrical properties and its operating conditions; the thermal performance in this case being centred on the heat transfer rates since most storage applications using PCM are facing a “rate problem”, *i.e.* heat transfer rates too low for the system to be fully optimised [19]. To this end, a three-dimensional numerical model taking into account heat transfer by

<sup>1</sup> To whom any correspondence should be addressed.

conduction in the PCM media, and heat transfer by conduction and convection in the air domain with laminar air flow was built and solved using the commercial finite element software, COMSOL Multiphysics 5.0.

The following section of this paper deals with a detailed description of the studied geometry, the mathematical model and the mesh sensitivity study. In the third section, the behaviour of the PCM during the melting process and the dependence of the heat transfer rate on the size of the cubic channels as well as the temperature and velocity of the incoming air are presented and discussed.

## 2. Methodology

### 2.1 Physical model

As described earlier, the studied geometry replicates a cellular air-to-air heat exchanger. However, every fresh incoming air channel was replaced with PCM, giving a checkerboard pattern. When hot extracted air flows through the heat exchanger, the heat is transferred to the PCM, leading to melting. When the stored heat would be required, a cold air stream would flow through the PCM-air heat exchanger to absorb the heat from the PCM. The entire geometry of the PCM-air heat exchanger is shown in Fig. 1a). Using symmetry considerations, only one PCM channel and 4 quarter channels (purple) and four half air channels (grey) needed to be simulated, as illustrated in Fig. 1b). Having an expected thermal conductivity much higher than the PCM, the heat exchanger thin walls were not modelled for simplicity in this work.

The PCM used for this study was dodecanoic acid, with a melting temperature of 43.5 °C. Tables 1 and 2 present the thermophysical properties of the PCM and air used in the simulations. The properties of dodecanoic acid were inputted manually into COMSOL; however, temperature dependent properties that were built into COMSOL were used for air. Inlet air temperatures of 60 °C and 70 °C were used in the simulation.

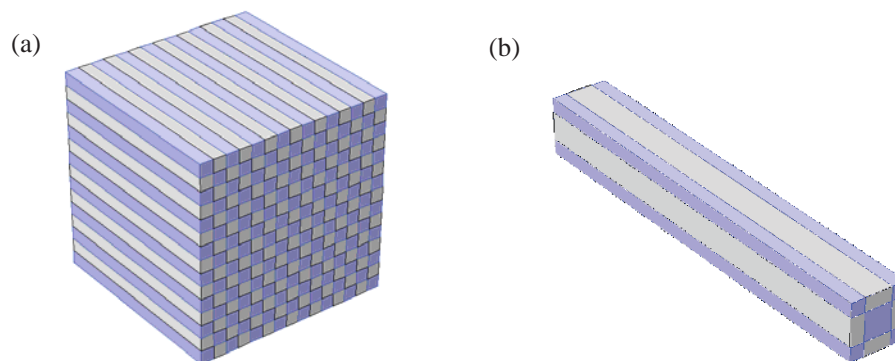


**Figure 1.** (a) The entirety of the PCM-air heat exchanger, (b) The geometry with symmetry used as the domain in the study.

**Table 1.** Thermophysical properties of dodecanoic acid [20].

Density	885 kg/m <sup>3</sup>
Heat Capacity (Solid)	2180 J/kg·K
Heat Capacity (Liquid)	2390 J/kg·K
Latent Heat of Fusion	187200 J/kg
Thermal Conductivity	0.15 W/m·K
Melting Point	43.5 °C

**Table 2.** Thermophysical properties of air.

	60 °C	70 °C
Density	1.060 kg/m <sup>3</sup>	1.029 kg/m <sup>3</sup>
Heat Capacity	1008 J/kg·K	1009 J/kg·K
Dynamic Viscosity	2.006×10 <sup>-5</sup> Pa·s	2.051×10 <sup>-5</sup> Pa·s
Thermal Conductivity	0.028 W/m·K	0.029 W/m·K

**Table 3.** List of varied parameters.

Channel edge length (cm)	Area of one inlet channel (m <sup>2</sup> ), $A_{air, ch}$	Number of air channels, $N_{air, ch}$	Heat transfer area (m <sup>2</sup> ), $A_{PCM-air}$	Inlet air temperature (°C)	Inlet air velocity (m/s)
6	0.0036	12	0.72	60, 70	0.75, 1
4	0.0016	28	1.26	60, 70	0.75, 1
2	0.0004	112	2.52	60, 70	0.75, 1

The system was studied by varying the dimension of the cubic PCM and air channel edges, from 2 to 4 to 6 cm, while their length stayed constant at 30 cm (refer to Fig. 1). The PCM domain had an initial temperature of 20 °C, while the inlet temperature of the air was varied between 60 °C and 70 °C. The inlet air velocity was varied between 0.75 m/s and 1 m/s assuming a laminar flow in the air domain. The largest Reynolds number being 3,180 for the largest channel and fastest flow and still considered mainly laminar for the purpose of this parametric study. The values of all parameters varied in this study are summarized in Table 3. Symmetry conditions were applied on the outside of the reduce domain. Through the changes in the edges length and inlet air temperature and velocity, the dependence of the heat transfer rate on the geometrical properties and the operating conditions could be determined.

## 2.2 Mathematical model

Within the PCM and air domains, the energy equation applies:

$$\rho C_p \frac{\partial T}{\partial t} + \nabla \cdot (-k \nabla T) + \rho C_p \mathbf{u} \cdot \nabla T = 0 \quad (1)$$

where the fluid velocity  $\mathbf{u}$  is always zero in the PCM domain and is determined from solving the Navier-Stokes equation for the air domain:

$$\begin{aligned} \frac{\partial \rho}{\partial t} + \nabla \cdot (\rho \mathbf{u}) &= 0 \\ \rho \frac{\partial \mathbf{u}}{\partial t} + \rho \mathbf{u} \cdot \nabla \mathbf{u} &= \nabla \cdot [\mu (\nabla \mathbf{u} + (\nabla \mathbf{u})^T)] - \nabla p \end{aligned} \quad (2)$$

The melting process can be modeled by modifying the overall heat capacity of the PCM to account for the large amount of energy provided by the latent heat of fusion,  $L$ , once the melting temperature,  $T_m$  is attained [21]. The resulting change in the specific capacity of the PCM during its melting is described by defining the two functions,  $B(T)$  and  $D(T)$  given by:

$$B(T) = \begin{cases} 0 & , T < (T_m - \Delta T/2) \\ \frac{T - T_m + \Delta T/2}{\Delta T} & , (T_m - \Delta T/2) < T < (T_m + \Delta T/2) \\ 1 & , T > (T_m + \Delta T/2) \end{cases} \quad (3)$$

$$D(T) = \frac{\exp[-(T - T_m)^2 / (\Delta T/4)^2]}{\sqrt{\pi}(\Delta T/4)} \quad (4)$$

$B(T)$  represents the liquid fraction in the PCM domain. Equation (3) shows that  $B(T)$  is equal to 0 in the solid phase, 1 in the liquid phase and varies linearly from 0 to 1 through the transition zone over a temperature interval,  $\Delta T$ .  $D(T)$  is a Gaussian function that accounts for the latent heat of fusion absorbed during the melting process. It has the value of zero everywhere except over the intervals  $(T_m - \Delta T/2)$  and  $(T_m + \Delta T/2)$ . More importantly, its integral over the range of all temperatures is equal to 1; therefore by multiplying  $D(T)$  by  $L$ , the energy balance through the phase transition is ensured.

Using the two functions described by Eqs. (3) and (4), the modified heat capacity,  $C_p(T)$ , of the PCM is defined as follows:

$$C_p(T) = C_{p,s} + B(T)(C_{p,l} - C_{p,s}) + L \cdot D(T) \quad (5)$$

where  $s$  and  $l$  refer to the solid and liquid phases of the PCM, respectively. More detail about this application of the modified heat capacity method can be found in [21]. It is important to note that

methods (both enthalpy and modified heat capacity) using a mushy zone for the modeling of phase change heat transfer on a fixed grid are not new [22] and have been well validated analytically and experimentally over the years. From solving the historical Stefan problem [23], to application in PCM composites [24] and melting with natural convection [25, 26] to name just a few studies out of hundreds.

### 2.3 Numerical resolution

The previously presented 3D geometry was created in COMSOL Multiphysics 5.0.; COMSOL along with ANSYS Fluent being two of the most used commercial software for phase change simulations worldwide [25]. The PCM and air properties given in Tables 1 and 2, along with the aforementioned initial and boundary conditions, were incorporated to the numerical model. The expressions of the liquid fraction,  $B(T)$ , and the Gaussian function,  $D(T)$ , were programmed within COMSOL through user-defined functions for a temperature interval,  $\Delta T$ , of 3 K. This temperature interval was selected to allow faster simulations on a less dense mesh, facilitating performing numerous simulations for this parametric study. The heat transfer in solid (PCM), in fluids (air) and the laminar flow (air) physics were implemented and coupled within COMSOL. This enabled the numerical modelling of conduction and convection within the system for the different geometrical properties and operating conditions listed in Table 3.

### 2.4 Mesh sensitivity study.

For the studied geometry, a swept quadrilateral mesh was used with an additional boundary layer mesh (4 layers) applied to the air domains (Fig. 2). A mesh independence study was performed in order to determine the appropriate size of elements to use, providing an accurate mesh independent solution and limiting the overall calculation time. To this end, two meshes were compared using  $16 \times 16 \times 40$  elements (Mesh 1) and  $32 \times 32 \times 80$  elements (Mesh 2), as shown in Fig. 2.

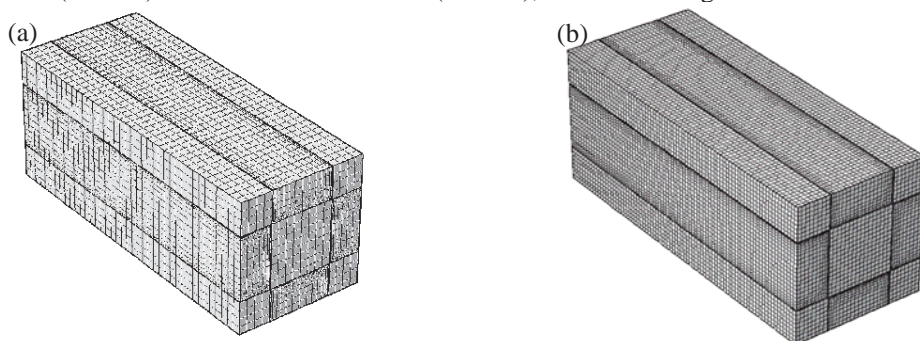


**Figure 2.** (a) Mesh 1 with  $16 \times 16 \times 40$  elements, (b) Mesh 2 with  $32 \times 32 \times 80$  elements.

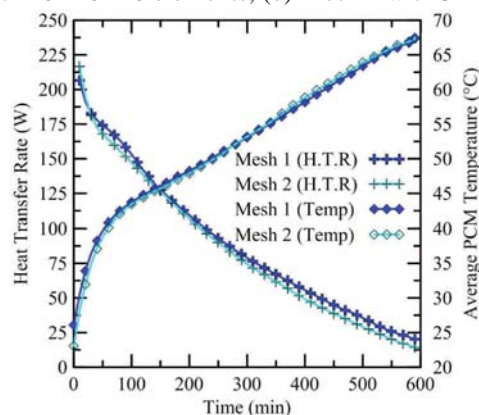


**Figure 3.** The average PCM temperature and the heat transfer rate as a function of time for the two studied meshes.

Figure 3 shows the average PCM temperature and the heat transfer rate as a function of time, for the two selected meshes, in the case of 6 cm channel size, 1 m/s inlet velocity, and 70 °C inlet temperature. It can be observed that the average PCM temperature profiles are almost overlapping for the two meshes, whereas the heat transfer rate obtained with the largest element number (Mesh 2) is slightly lower compared to the one resulting from Mesh 1. From this result, and since the goal of this work is to present a parametric study, the level of accuracy and simulation time saving obtained from Mesh 1 leads to the conclusion that appropriate mesh independence was obtained. Therefore, a total number of 21480 (16×16×40) quadrilateral elements will be used in the study.

### 2.5 Resolution Procedure

In total, 12 simulations were completed for 10 simulated hours each. The computation time varied between 4 hours and 27 hours for the configurations when running on a workstation with 32 cores clocked at 2.4 GHz and 128 GB of RAM.

### 3. Results and discussion

As previously mentioned, this study explores the dependence of the heat transfer rate on inlet air velocity and temperature as well as the channel size in a cubic PCM-air heat exchanger. The heat transfer rate,  $Q$ , is defined by Eq. (6), where  $A_{air, ch}$  is the cross sectional area of one air channel and  $N_{air, ch}$  is the number of air channels in the full 30×30×30 cm<sup>3</sup> heat exchanger (see Table 3);  $\rho$ ,  $C_p$  and  $v_{in}$  are the density, heat capacity and velocity of the incoming air respectively, and  $(T_{in, air} - T_{out, air})$  is the difference between the inlet and outlet air temperatures. The heat transfer rate is driven by the outlet temperature which is calculated through the transient simulation in COMSOL, as the other parameters vary only slightly over 10 hours of simulation time.

$$Q = A_{air, ch} \cdot N_{air, ch} \cdot \rho \cdot C_p \cdot v_{in} \times (T_{in, air} - T_{out, air}) \quad (6)$$

From Eq. (6), the heat flux at the air-PCM interface is defined as:

$$q'' = Q/A_{PCM-air} \quad (7)$$

where  $A_{PCM-air}$  is the total surface area of the air-PCM interface for the entire 30×30×30 cm<sup>3</sup> heat exchanger (see Table 3).

Figures 4 to 11 display the simulated heat transfer rate, heat flux, average PCM temperature (taking over the entire PCM volume) and melt fraction, for all the parameter combinations between channel size, inlet air velocity and temperature (Table 3). The figures on the left display varying channel sizes and inlet velocities for an incoming air temperature of 60 °C, while the figures on the right display the same configurations but for an incoming air temperature of 70 °C.

Several observations can be made from Figs. 4 and 5. First, the initial heat transfer rate is higher with 70 °C incoming air but decays more quickly than in the 60 °C simulations. This is expected as the temperature differential between the 70 °C air and 20 °C PCM is greater, so the heat transfer rate is expected to be greater as well. The system reached equilibrium more quickly because the PCM melted more quickly, as can be seen from the transient evolution of the melted PCM fraction shown in Figs. 10 and 11. Secondly, the size of the channels made the biggest difference in the heat transfer rate. In both 60 °C and 70 °C simulations, the 2 cm channel size started at twice the heat transfer rate of the 4 cm channel size but decayed a lot more quickly. Again, this follows the accelerated melting of the PCM in the 2 cm channel simulations (Figs. 10 and 11). Overall, the 2 cm channel size system offer the largest heat transfer area which explains the larger heat transfer rate.

For all channel sizes and inlet temperatures, the 1 m/s inlet velocity started out as the configuration with the highest heat transfer rate, but the 0.75 m/s inlet velocity overtook it later in the simulation. The cross-over occurred increasingly later in the simulation as the channel sizes became larger.



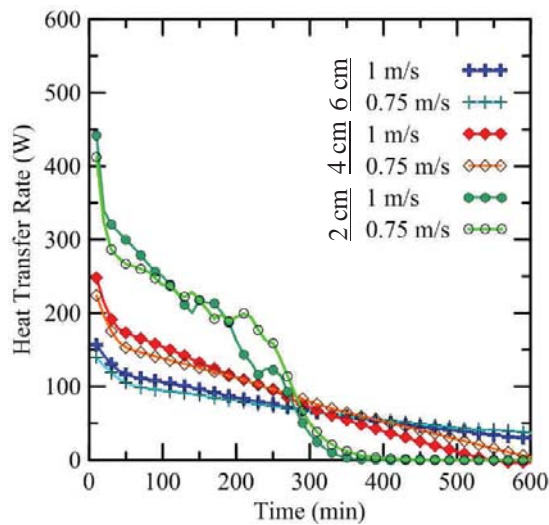


**Figure 4.** Heat transfer rate between 60 °C air and PCM.

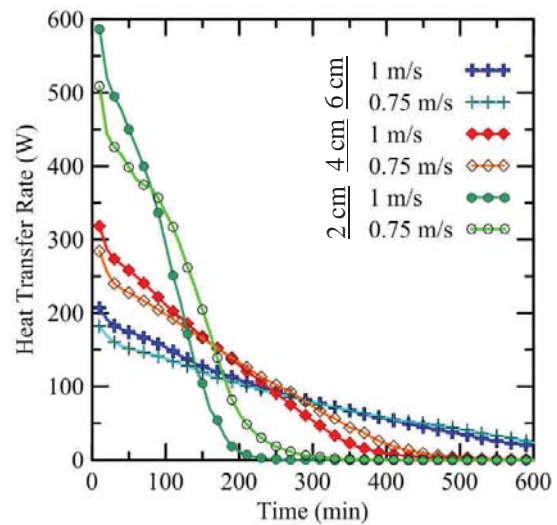


**Figure 5.** Heat transfer rate between 70 °C air and PCM.

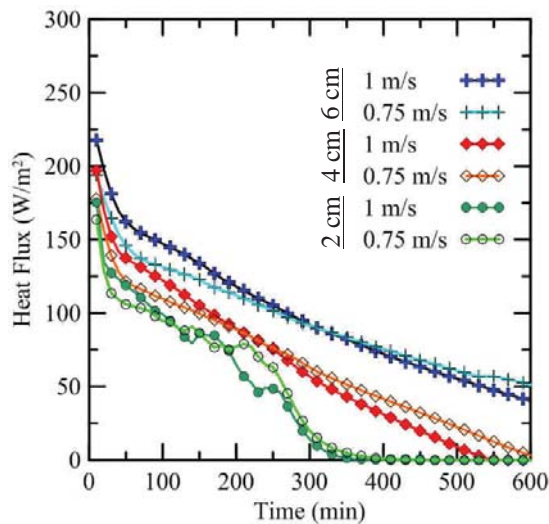


**Figure 6.** Heat flux for 60 °C in-flow.

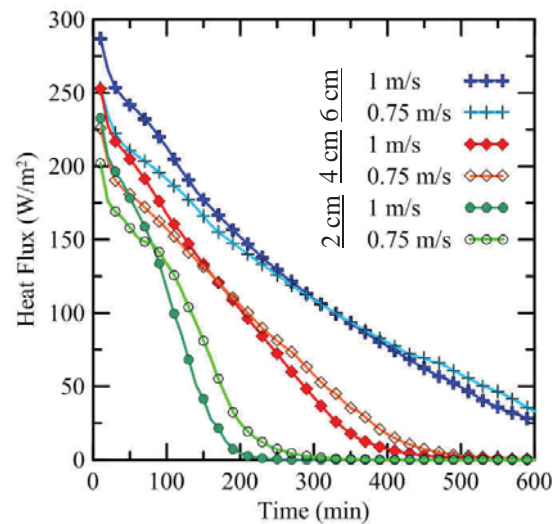


**Figure 7.** Heat flux for 70 °C in-flow.

The slight fluctuations in the 2 cm channel size in the 60 °C simulations were most likely due to numerical instabilities, which may be a result of not achieving full mesh convergence for the smaller channel sizes; more elements might have been required. However, due to time constraints and for consistency, the mesh for the 2 cm had to have the same number of elements as the other channel sizes.

The heat flux between the air and PCM interfaces did not follow exactly the same pattern as the heat transfer rate. All channel sizes started at roughly the same value in both the 60 °C and 70 °C simulations. Interestingly, the smaller channel offered a slightly lower heat flux (the opposite trend compared to the heat transfer rate results); this can be explained by the fact that with larger channel, the temperature profile in the air in the channel leads to a greater temperature difference between the wall and the centerline, hence a higher temperature gradient at the wall. Also, as in the heat transfer rate graphs, the smaller the channel size, the more quickly the heat flux decayed to zero. Not surprisingly, the 70 °C simulations (Fig. 7) started at a higher heat flux than the 60 °C simulations (Fig. 6), which is a direct result of the greater temperature differential. And again as in the heat transfer rate graphs, the effect of velocity was the same.

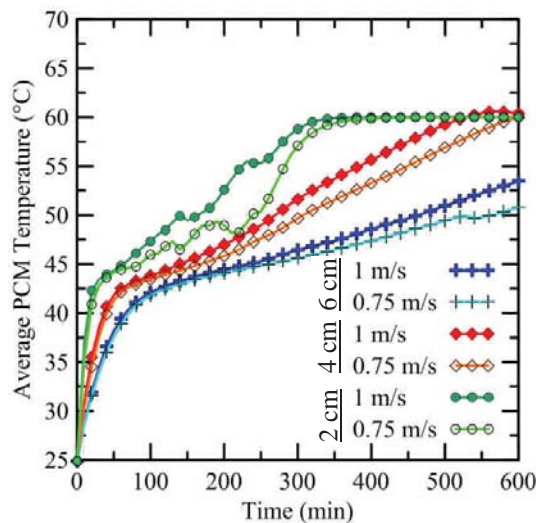


**Figure 8.** PCM temperature for 60 °C in-flow.

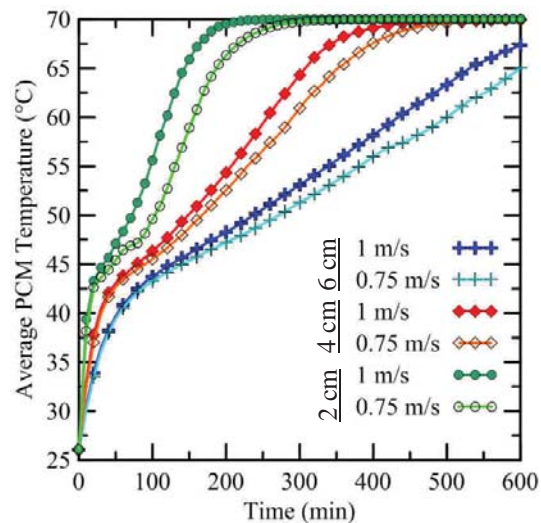


**Figure 9.** PCM temperature for 70 °C in-flow.

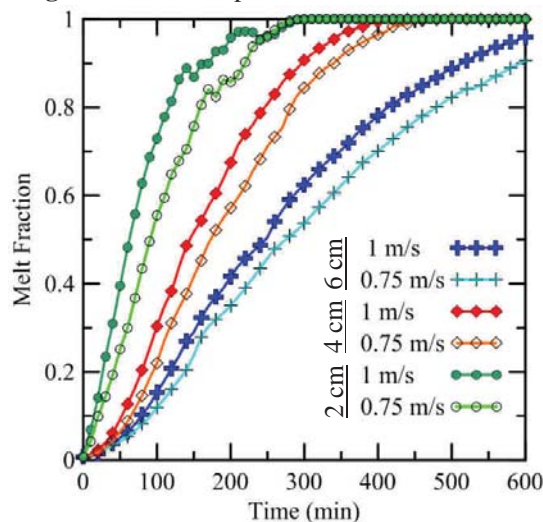


**Figure 10.** Melt fraction for 60 °C in-flow.

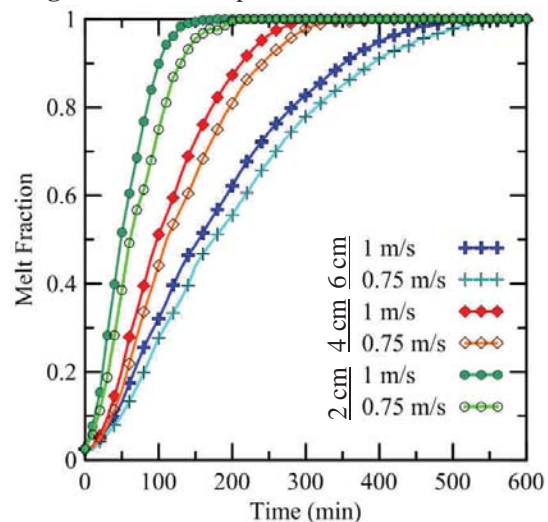


**Figure 11.** Melt fraction for 70 °C in-flow.

When studying the average temperature of the PCM, it is possible to observe the levelling off of temperature around the melting point of the dodecanoic acid (43°C) in Figs. 8 and 9, which is a manifestation of the latent heat component of the PCM. As shown in Fig. 10 (60 °C), the PCM melted completely after approximately 300 minutes of simulation time for the 2 cm channel sizes and after 500 minutes of simulation time for the 4 cm channel sizes. The PCM did not fully melt with the 6 cm channel sizes after 600 minutes of simulation time. In Fig. 11 (70 °C), the PCM fully melted approximately 100 and 200 minutes before the 60 °C simulations for the 2 cm and 4 cm channel sizes respectively. The 6 cm channel size led to nearly complete melting at the very end of the simulation.

As discussed previously, the 1 m/s inlet velocity resulted in slightly higher heat transfer rates in the beginning of the simulations. This impact is reflected in the average PCM temperatures and melt fractions in Figs. 8 to 11.

#### 4. Conclusion

This paper studied the effect that the geometry and operating conditions of a PCM-air heat exchanger had on the heat transfer rate between the incoming hot air and dodecanoic acid. Through 10 hour long

simulations conducted in COMSOL Multiphysics 5.0, it was determined that the configuration with a channel size of  $2 \times 2 \times 30 \text{ cm}^3$ , inlet velocity of 1 m/s, and inlet temperature of  $70^\circ\text{C}$  resulted in the highest heat transfer rate at the beginning of the 10 hour simulation and the sharpest rate of decline. Conversely, the configuration with a channel size of  $6 \times 6 \times 30 \text{ cm}^3$ , inlet velocity of 0.75 m/s, and inlet temperature of  $60^\circ\text{C}$  resulted in the lowest heat transfer rate between the incoming air and the PCM in the beginning of the simulation but also the slowest rate of decline over the length of the simulation. Within the configurations studied in these simulations, the size of the channels had the biggest effect on the heat transfer rate between the air and PCM, followed by the incoming air temperature. The inlet velocity had the smallest effect. However, the actual heat flux from the air to the PCM was greater for the larger channel size, due to the larger temperature gradients observed at the wall.

In this sense, the former PCM-air configuration ( $2 \times 2 \times 30 \text{ cm}^3$  channels, inlet velocity of 1 m/s, and inlet temperature of  $70^\circ\text{C}$ ) is the most efficient as the PCM achieves complete melting quicker, hence faster thermal storage which is often needed in thermal storage applications.

### Acknowledgements

The authors would like to thank Public Work and Government Services Canada (PWGSC), the Natural Science and Engineering Research Council (NSERC) of Canada and the Canada Foundation for Innovation (CFI) for their financial support.

### References

- [1] Vakilaltojjar S M and Saman W 2001 *Appl. Therm. Eng.* **21** 249-263.
- [2] Zalba B, Marín J M, Cabeza L F and Mehling H 2004 *Int. J. Refrig.* **27** 839-849.
- [3] Hed G and Bellander R 2006 *Energy Build.* **38** 82-89.
- [4] Lazaro A, Dolado P, Marin J M and Zalba B 2009 *Energy Convers. Manag.* **50** 444-449.
- [5] Dolado P, Lazaro A, Marin J M and Zalba B 2011 *Energy Convers. Manag.* **52** 1890-1907.
- [6] Gowreesunker B L, Tassou S A and Kolokotroni M 2013 *Build. Environ.* **65** 132-145.
- [7] Arzamendia Lopez J P, Kuznik F, Baillis D and Virgone J 2013 *Energy Build.* **64** 415-422.
- [8] Mosaffa A H, Infante Ferreira C A, Talati F and Rosen M A 2013 *Energy Convers. Manag.* **67** 1-7.
- [9] Labat M, Virgone J, David D and Kuznik F 2014 *Appl. Therm. Eng.* **66** 375-382.
- [10] Kuznik F, Arzamendia Lopez J P, Baillis D and Johannes K 2015 *Energy Build.* **106** 65-73.
- [11] Mankibi M E, Stathopoulos N, Rezaei N and Zoubir A 2015 *Energy Build.* **106** 74-86.
- [12] Dubovsky V, Ziskind G and Letan R 2011 *Appl. Therm. Eng.* **31** 3453-62.
- [13] Ezra M, Kozak Y, Dubovsky V and Ziskind G 2016 *Appl. Therm. Eng.* **93** 315-329.
- [14] Omojaro P and Breitung C 2014 *Energy Procedia.* **48** 413-422.
- [15] Antony Aroul Raj V and Velraj R 2011 *Int. J. Therm. Sci.* **50** 1573-1582.
- [16] Tay N H S, Belusko M and Bruno F 2012 *Energy Build.* **50** 234-242.
- [17] Arkar C, Vidrih B and Medved S 2007 *Int. J. Refrig.* **30** 134-143.
- [18] O'Connor D, Calautit J K S and Hughes B R 2016 *Renew. Sustain. Energy Rev.* **54** 1481-93.
- [19] Groulx D, C Kheirabadi A, Desgrosseilliers L, Kabbara M, Azad M, Donaldson A, Joseph A and White M A 2016 *INNOSTORAGE Conf.* Ben-Gurion University of the Negev Beer-Sheva Israel.
- [20] Desgrosseilliers L, Whitman C A, Groulx D and White M A 2013 *Appl. Therm. Eng.* **53** 37-41.
- [21] Groulx D and Biwole P H 2014 *Proc. of the 15th Int. Heat Transfer Conf. IHTC-15* Kyoto Japan
- [22] Voller V R and Prakash C 1987 *Int. J. Heat Mass Transfer* **30** 1709-1719
- [23] Ogoh W and Groulx D 2010 *6<sup>th</sup> Annual COMSOL Conference*, Boston USA
- [24] Mallow A M, Abdelaziz O and Graham Jr S 2016 *1<sup>st</sup> Pacific Rim Thermal Engineering Conference*, Hawaii USA.
- [25] C Kheirabadi A and Groulx D 2015 *Advances in Computational Heat Transfer CHT-15*, Rutgers University Piscataway USA
- [26] Biwole P H, Eclache P and Kuznik F 2013 *Energy Build* **62**, 59-67